Soil Structure Interaction Effects on Stability of HP/HT Unburied Subsea Pipelines Using a Probabilistic-Based Approach

Davide Forcellini (dfor295@aucklanduni.co.nz)
University of Auckland https://orcid.org/0000-0003-1253-8572
Daniele Mina
Griffith University - GC Campus: Griffith University - Gold Coast Campus
Hassan Karampour
Griffith University - GC Campus: Griffith University - Gold Coast Campus

Original Article

Keywords: SSI, PIPELINES, seismic, INTERACTION

Posted Date: February 5th, 2021

DOI: https://doi.org/10.21203/rs.3.rs-162915/v1

SOIL STRUCTURE INTERACTION EFFECTS ON STABILITY OF HP/HT UNBURIED SUBSEA PIPELINES USING A PROBABILISTIC-BASED APPROACH

Davide Forcellini[1] Daniele Mina[2] and Hasan Karampour[2]

[1]Dr., Civil and Environmental Engineering Department, University of Auckland, Auckland, New Zealand (corresponding author), dfor295@aucklanduni.co.nz

[2]School of Engineering and Built Environment, Griffith University, Gold Coast, QLD, Australia,

ABSTRACT

Soil structure interaction (SSI) may considerably affect the seismic vulnerability of subsea high pressure/high temperature (HP/HT) pipelines. Numerical simulations are herein proposed to study the effects of soil deformability on failure of an unburied pipeline with D/t = 20, laid on the seabed and resting on a sleeper. OpenSees is used to assess an earthquake scenario imposed on a laterally buckled pipeline by considering the effects of non-linear soil behaviour on the mechanisms that induce damage on the soil-pipeline system. Uncertainties in the case study were considered by applying a probabilistic-based approach and by developing analytical fragility curves that allow estimation of the probability of exceedance of the selected failure criteria.

INTRODUCTION

Assessing the seismic vulnerability of critical infrastructures is fundamental in order to allocate resources toward their design and maintain a certain level of functionality for the societies. Since pipelines are important networks for servicing communities with water, sewage, oil and natural gas,

decision makers need to carefully preserve their serviceability and resilience. In this regard, buckling is one of the most critical conditions that can lead to severe failure for pipelines and thus was investigated in the 30 years. For example, Yun and Kyriakides (1990) considered the effects of compressive loads due to soil deformability and Dyan and Kyriakides (1992) analysed the combination of bending and tension by applying a 2D model. Vazouras et al. (2010, 2012, 2015) performed several parametric studies to assess the axial strains and displacements of pipelines. Recently Mina et al. (2020) developed fragility curves that account for the interaction between buckling and earthquakes and Triantafyllaki et al. (2020) performed 3D numerical simulations of a partially embedded (unburied) pipeline in to assess its vulnerability to a fault rupture. Other authors (such as Karampour et al. (2018, 2015), Alrzai and Karampour (2016), Binazir et al. (2019), Stephan et al. (2016) and Piran at al. (2020) investigated the stability of subsea pipelines and pipe-in-pipe systems under hydrostatic, hydrodynamic, thermal and combined actions. However, very few contributions have considered the effects of SSI on unburied pipelines that have been performed with finite element models. The surrounding soil have been reproduced with several approaches by applying non-linear translational springs Joshi et al. (2011), Liu et al. 82004 and 2008), Odina and Tan (18) and Odina and Conder (2010) or 3D solid elements Kokavessis and Anagnostidic (2006). In particular, Joshi et al. (2011) applied beam elements for the pipeline and discrete nonlinear springs for the soil by deriving an analytical solution for the equivalent springs at the pipeline ends. The role of soil deformability was considered by Zhang et al. (2014) that proposed a finite element model considering ground-pipeline interaction in soil and rock layers and by Thebian et al. (2017) that investigated the role of fault displacements on the buckling mechanism of buried offshore pipelines in sandy soils.

In particular, the mutual soil–pipe interaction may have important effects on the pipeline response, as shown in (2009). Kokavessis and Anagnostidis (2006) applied contact elements to describe the SSI while Karamitros et al. (2007) performed a combination of beam-on-elastic-foundation and beam theories. Liu et al. (2004) performed a finite element model that applies a combination of shell elements and springs to predict the axial strain along the pipeline. Shitamoto et al. (2010) proposed to model the pipeline with a solid-element model to study strain conditions induced by soil liquefaction. Arifin et al. (2010) and Odina (2009 and 2010) modelled the soil with nonlinear springs while more recently Daiyan et al. (2010) applied elasto-plastic 3D solid finite elements to investigate the soil–pipe interaction. In order to address the gap in literature, the current work aims to develop a model based on a previous recent work Mina et al. (2020) and provide more insight into the failure of a subsea pipeline by investigating the effect of soil properties.

NUMERICAL MODEL

Mina et al. 2020 investigated the vulnerability of subsea high pressure/high temperature (HP/HT) pipelines to seismic actions. They modelled a pipeline laid on the seabed and resting on a sleeper as shown in Fig. 1, with parameters represented in Table 1. Two scenarios were analysed: in scenario 1, the earthquake input was imposed on a laterally buckled pipe, and in scenario 2, the seismic motion was applied at a temperature slightly below the lateral buckling temperature. By developing analytical fragility curves, Mina et al. [8] showed that the probability of failure (exceedance of the yield stress or local buckling of the pipe wall-thickness) is higher in scenario 1. In the current study the same pipeline model with scenario 1 is considered and different input motions are applied to the soil.

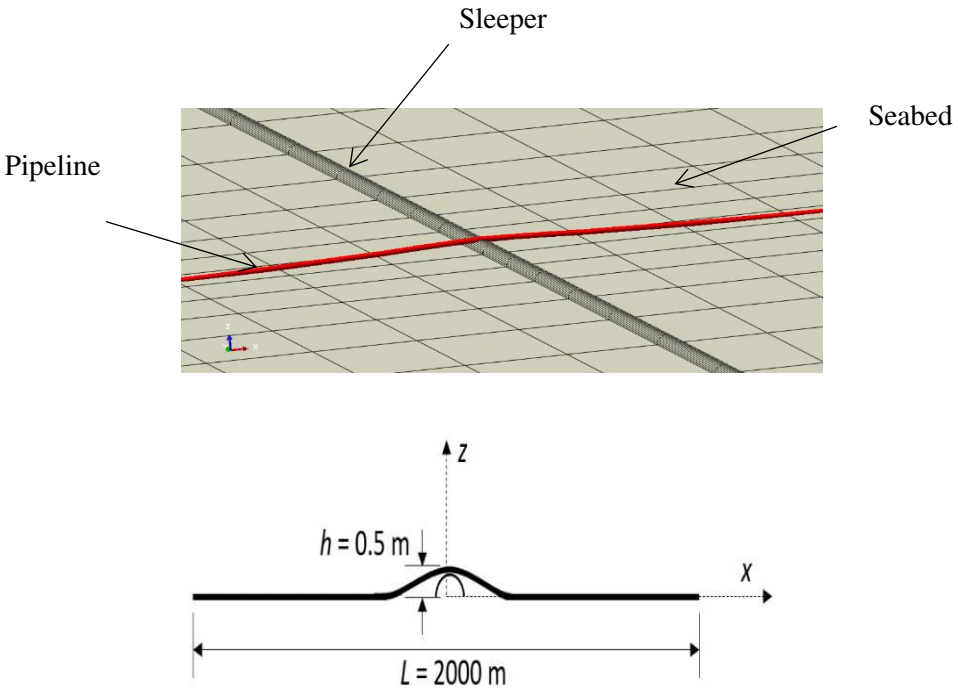

Fig. 1. Pipeline and sleeper model used in the thermal buckling and seismic/thermal interaction analyses in Mina et al. (2020).

The soil (Fig. 2) is modelled with a 200 x 200 m x 20 m 3D mesh built up with 6360 nodes and 5330 non-linear *Bbar brick* elements (Lu et al., 2011 and Mazzoni et al., 2009) . For each element 20 nodes describe the solid translational degrees of freedom (DOF) and for each of them DOFs 1, 2 and 3 represent solid displacement recorded using OpenSees Node Recorder at the corresponding integration points (Mazzoni et al., 2009). The number of elements is defined on the basis of the wavelength of the seismic signal and the maximum frequency above which the spectral content of

79 the input can be considered negligible. Dimensions of the elements are increased from the centre of
80 the mesh to the lateral boundaries, which are modelled to behave in pure shear and located far away
81 (more details in Forcellini, 2020a). The mesh quality was tested by verifying that the accelerations
82 on the surface near the lateral boundaries were identical to those simulating free-field conditions.
83 Penalty method (tolerance: 10^{-4} Mazzoni et al., 2009), is applied at the lateral boundaries and shear
84 deformations are allowed by setting the longitudinal and transversal directions unconstrained.
85 Vertical direction is fixed on the lateral boundaries and at the base. In order to simulate the behaviour
86 of a 2000 m-long pipeline, the boundary conditions are modelled by defining a zero-length element
87 at each end of the pipeline in all three directions. In the longitudinal and transversal directions, non-
88 linear properties were defined on the basis of an elastic perfectly plastic (EPP) backbone curve
89 representing the pipeline resistance. In the vertical direction, an elastic spring is defined at each end
90 of the pipeline with a stiffness corresponding to the vertical stiffness of the soil.

91

92 **Table 1.** Pipeline and seabed properties, Mina et al. (2020)

Length, L (m)	2000
Outer diameter, OD (mm)	254
Wall thickness, t (mm)	12.7
Thermal expansion coefficient, α (°C^{-1})	$1.01 \cdot 10^{-5}$
Young's modulus, E (MPa)	206000
Poisson's ratio, v	0.3
Lateral imperfection ratio, h_0/l_0	0.012
Submerged weight, q (N/m)	1500
Seabed friction coefficient, μ_1	0.5
Sleeper friction coefficient, μ_2	0.3
Sleeper height, h (m)	0.5

93

94 Three homogeneous soil layers (named STIFF, MEDIUM and SOFT) with increasing deformability
95 were performed in order to consider the non-linear effects of the soil, such as amplitude-dependent
96 amplification (or deamplification), plastic accumulations of ground deformation and permanent
97 movements (rotations, settlements and tilts) at the foundation level. The *Pressure Independent Multi-*
98 *Yield* (PIMY) model (representative parameters shown in Table 2) was applied in order to consider
99 the non-linear mechanisms of hysteretic response and radiation damping. PIMY implements the Von
100 Mises multi-surface kinematic plasticity model allowing to control the cycle-by-cycle mechanism of

permanent shear strain accumulation (Lu et al., 2011). In particular, the deviatoric part of the flow rule is associated (non-linear) and independent from the volumetric part (non-associated and linear-elastic). A more detailed description is found in Lu et al. (2011). The non-linear back-bone curves are represented by hyperbolic relations and are defined by the shear strain modulus and the ultimate shear strength (Fig. 3).

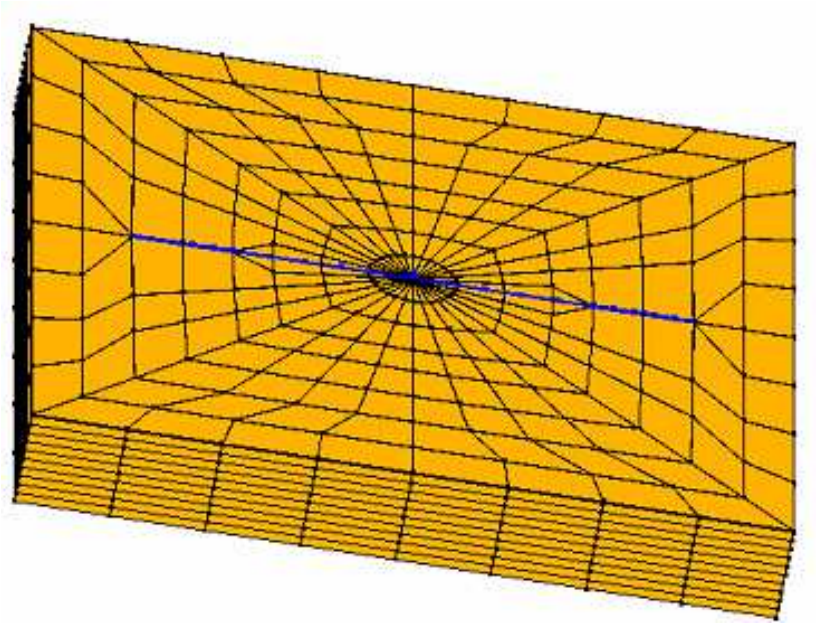

Fig. 2. The finite element mesh

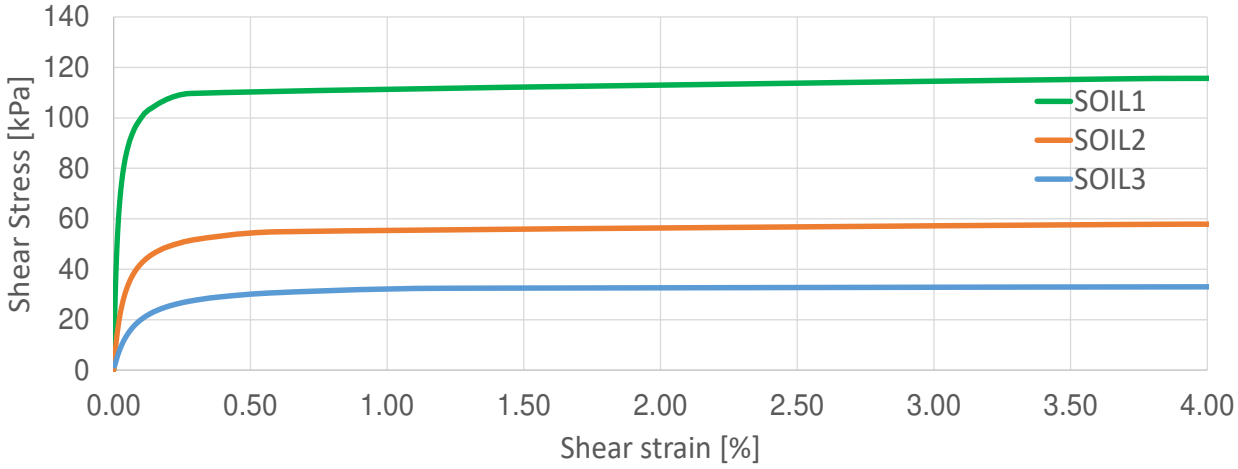

Fig. 3. Backbone curves

Table 2 - Soil parameters

	SOIL1	SOIL2	SOIL3
Mass density (Mg/m^3)	2.0	1.7	1.5
Shear Modulus (kPa)	$7.2 \cdot 10^5$	$1.53 \cdot 10^5$	$6 \cdot 10^4$
Bulk Modulus (kPa)	$1.56 \cdot 10^6$	$3.32 \cdot 10^5$	$3 \cdot 10^5$
Cohesion (kPa)	100	50	37
Shear wave velocity (m/s)	600	300	200

Following Mina et al. 2020, the thermal buckling response of the pipeline was reproduced with several load steps, by applying a quasi-static dynamic analysis (geometric nonlinearity was included), and by considering the buckled configuration, namely scenario 1. The following load steps and in the mentioned order were applied: (1) a distributed mass of 153 kg/m representing the self-weight (including the submerged weight of the pipeline and its concrete coating), (2) the internal pressure (P_{int} = 12 MPa) and (3) a uniform temperature of 31°C applied to the wall thickness.

As shown in Karampour et al. (2013) and Karampour (2018) the lateral buckling depends on the axial forces in the wall thickness that occur as a consequence of the soil reaction to the expansion of the pipeline when subjected to the internal pressure and thermal loading. In this regards, simulating SSI becomes fundamental to realistically predict such conditions that may severely damage the pipeline.

The seismic inputs are applied to the soil domain in the transversal direction at a depth of 25 m. In order to calculate the bending response, the pipeline was modelled as an isotropic bilinear material (yield stress σ_y = 448 MPa and tangent modulus E_t = 2100 MPa). The strains are calculated at the central point, at the crown of the buckled pipeline (Mina et al. 2020), and then compared against the failure criteria outlined in the next section.

PIPELINE FAILURE CRITERIA

DNV (2007) outlines the local buckling under combined loading failure criteria. For a pipeline subjected to longitudinal compressive strain induced by bending moment, axial force and internal overpressure (internal pressure in excess of the external hydrostatic pressure), the following design condition should be satisfied at all cross-sections:

$$\varepsilon_{Sd} \leq \varepsilon_{Rd} = \frac{\varepsilon_c}{\gamma_\varepsilon} \tag{1}$$

$$\varepsilon_c = 0.78\left(\frac{t}{D} - 0.01\right)\left(1 + 5\frac{p_i - p_e}{p_b \cdot \frac{2}{\sqrt{3}}}\right)\alpha_h^{-1.5}\alpha_{gw} \quad (2)$$

where ε_{Sd} is the design compressive strain, p_i and p_e are the internal and external pressures, respectively, and γ_ε is the resistance strain factor. The burst pressure p_b is calculated from:

$$p_b = \frac{2t}{D-t} f_Y \frac{2}{\sqrt{3}} \quad (3)$$

The strain hardening parameter α_h is equal to 0.93 for C-Mn steel pipe (DNV, 2007) and the girth weld factor (α_{gw}) is equal to 1 with D/t = 20. For the pipe studied herein with parameters represented in Table 1, ε_c is equal to 6.1×10^{-2} mm/mm. The resistance strain factor γ_ε for 3 different classes low, medium and high are equal to 2.0, 2.5 and 3.3, respectively (DNV, 2007). The design compressive strain ε_{Sd} for different classes are represented in Table 3. The strain at failure (local buckling of the compressive side) from the FE analysis (Mina et al., 2020) is also given in Table 3.

Table 3. Failure criteria for different safety classes

			ε_{Sd} (mm/mm)			
OD (mm)	t (mm)	f_Y (MPa)	Low safety class	Medium safety class	High safety class	FEA [8]
254	12.7	448	3.0×10^{-2}	2.44×10^{-2}	1.85×10^{-2}	1.58×10^{-2}

Fragility curves were applied in order to consider a probabilistic-based methodology to assess the role of soil deformability on the behaviour of HP/HT unburied subsea pipelines, as previously applied in Mina et al. (2020), Forcellini (2020b and 2021). In particular, the proposed fragility curves were developed as to represent the relationships between the conditional probability of exceeding predefined limit states (LS) for given levels of the maximum strains in Table 3 in the compression at the crown of the pipeline used as the reference engineering demand parameter (EDP). Therefore, the lognormal standard deviation (β) and the mean (μ) of the lognormal peak ground acceleration (PGA), used as the reference intensity measure were calculated (Mina et al. 2020) in order to develop fragility curves.

RESULTS AND DISCUSSION

In this section, the FE model is firstly validated by comparing the results with the ones calculated in the previous paper (Mina et al, 2020) for the case of SOIL1. The results (bedrock conditions, Fig. 4) show a good agreement, meaning that the model assumptions were properly defined. The conditions of rigid soil (no SSI) were compared with the other soil conditions.

Therefore, the results from the 300 (100 for the 3 soil conditions) dynamic analyses were represented in order to build linear regression and define the mean and log-standard deviation values. Fig. 5 shows the results for the three soil conditions and the mean and the lognormal standard deviation values are plotted in Table 4-6. It is worth noting that deformable soils (SOIL2 and SOIL3) show smaller mean values than those for SOIL1, underlining the effect of soil deformability in reducing the seismic vulnerability of the soil-pipeline system.

In particular, Figs. 6-8 show that for SOIL1 and SOIL2 the curves for the various limit states differ more than those for SOIL3, where the probability of exceedance (PE) is high even at slight and moderate level of damage. The performance of the system (soil and pipeline) is shown to be characterized by different levels of PE and, consequently, damage for SOIL2 and SOIL3. SOIL1 represents the case of a stiff soil (bedrock conditions) and thus it may be assumed that SSI effects are negligible (fixed conditions). This aspect may lead to the fact that the pipeline strains are not due to the soil residual plastic deformations, as show in Mina et al. (2020).

Figs. 9 and 10 compare the considered soil conditions for LS1 and LS4, respectively. For example, at 0.30*g* (Table 7), PE values for LS1 are 0.77, 0.80 and 0.84, while for LS4 PE values are 0.68, 0.70 and 0.79, respectively for SOIL1, SOIL2 and SOIL3. In particular, Figs. 9 and 10 show that the pipeline vulnerability increases with soil deformability, since the PE for SOIL1 is reduced across the entire range of PGA for all the damage states, if compared with SOIL2 and SOIL3. It is worth noting the difference of the probability reached at LS4 for SOIL2 and SOIL3. This difference is relatively small for motion with PGA < 0.20*g* and for PGA > 0.30*g*. The difference increases gradually between 0.20*g* and 0.30*g* and at 0.24*g* the PE values are 0.60 and 0.70 for SOIL2 and SOIL3, respectively. The difference between the two soil conditions decreases for higher intensities and, for example, at 0.70*g* PE values are 0.97 and 0.94. This is due to non-linear deformations in the soils that become significant after a certain level is reached. In particular, the non-linear behaviour of the soil is driven by the ultimate strength of the soil (defined by the backbone curves, Fig. 2) that needs a certain level of intensity to be mobilized. For SOIL3, the final shear strength (38 kPa, Fig. 2) may be reached for intensity levels that are lower than those for SOIL2 (59.8 kPa, Fig. 2). Therefore, the relative damage

of the two soil conditions differ mainly at moderate level of PGA because such intensities may affect the soil in different ways. At higher level of PGA, the soil mobilize plastic behaviour and the performance of the soil-pipeline system is similar. Figs. 7 and 8 show that when SSI is considered, the curves shift toward more fragile behaviour due to damage that is induced by the presence of the soil. This increased vulnerability is evident for LS4, where SOIL3 shows larger values of PE, demonstrating that SSI effects are detrimental. Particularly, the effects of soil damping is also fundamental (see Forcellini, 2021).

Overall, the paper shows how the strains due to scenario 1 (Mina et al., 2020) may considerably be amplified when soil deformation is considered. It was shown that neglecting the SSI effects on the performance of the system (SOIL1 conditions) may considerably undervalue the pipeline vulnerability, leading to un-conservative predictions and designs. The proposed findings may be included in code provisions to consider the role of SSI with a probabilistic-based approach.

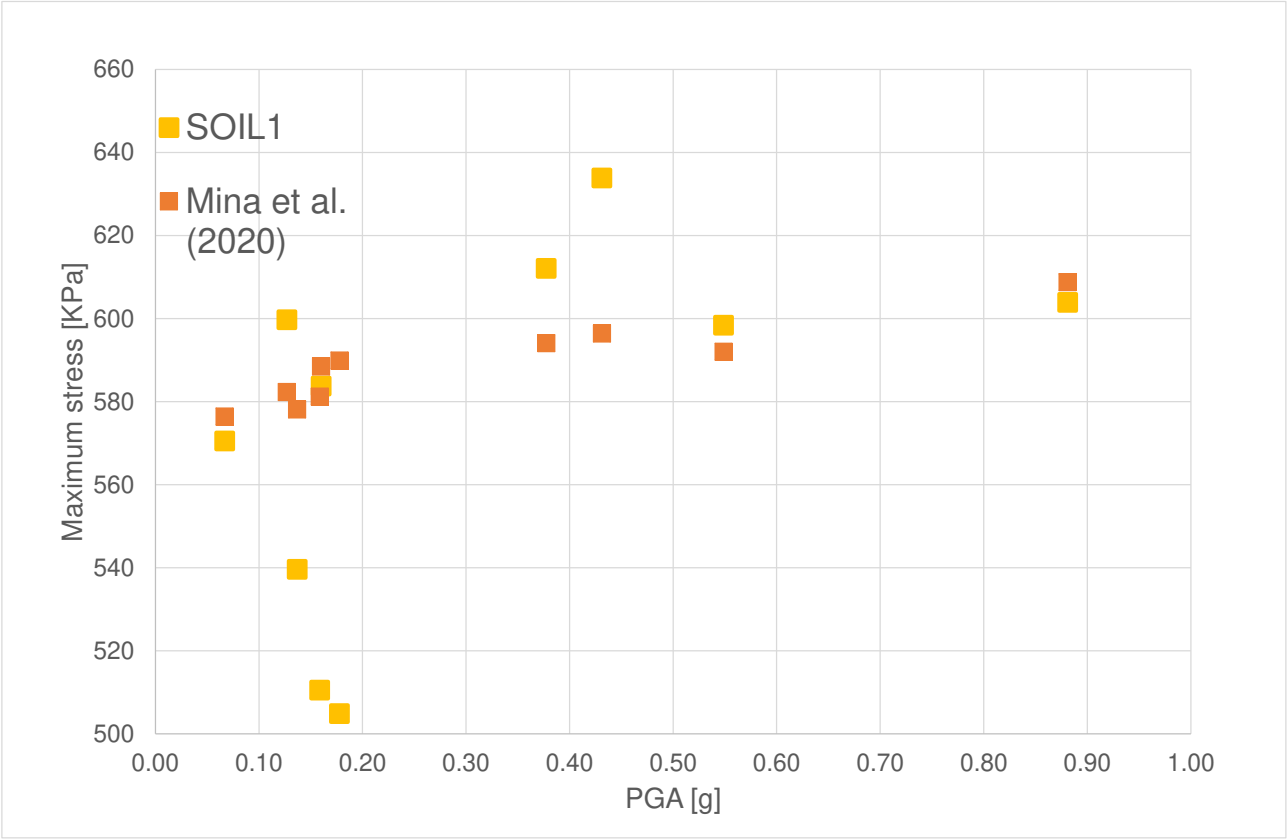

Fig. 4. Comparison: Mina et al. (2020) and Soil 1 results

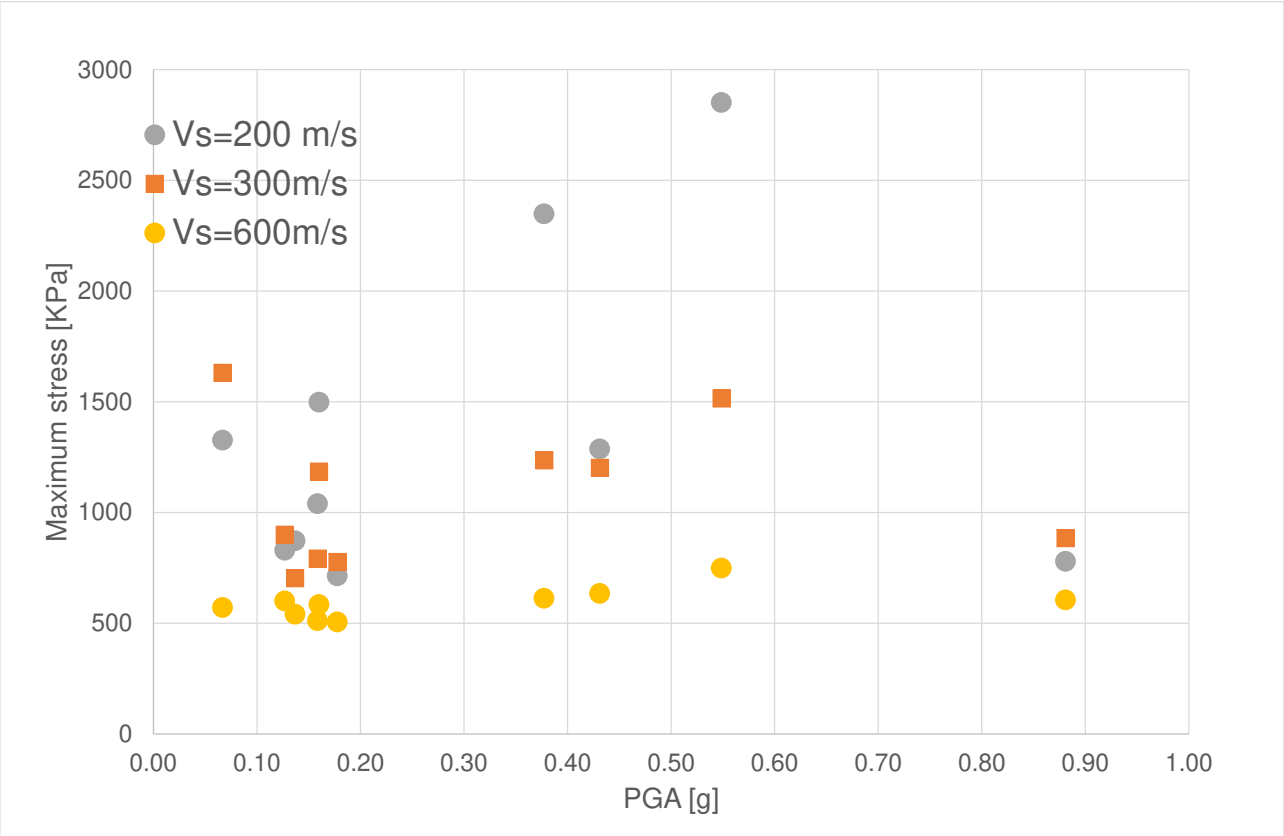

Fig. 5. Comparison: SSI effects

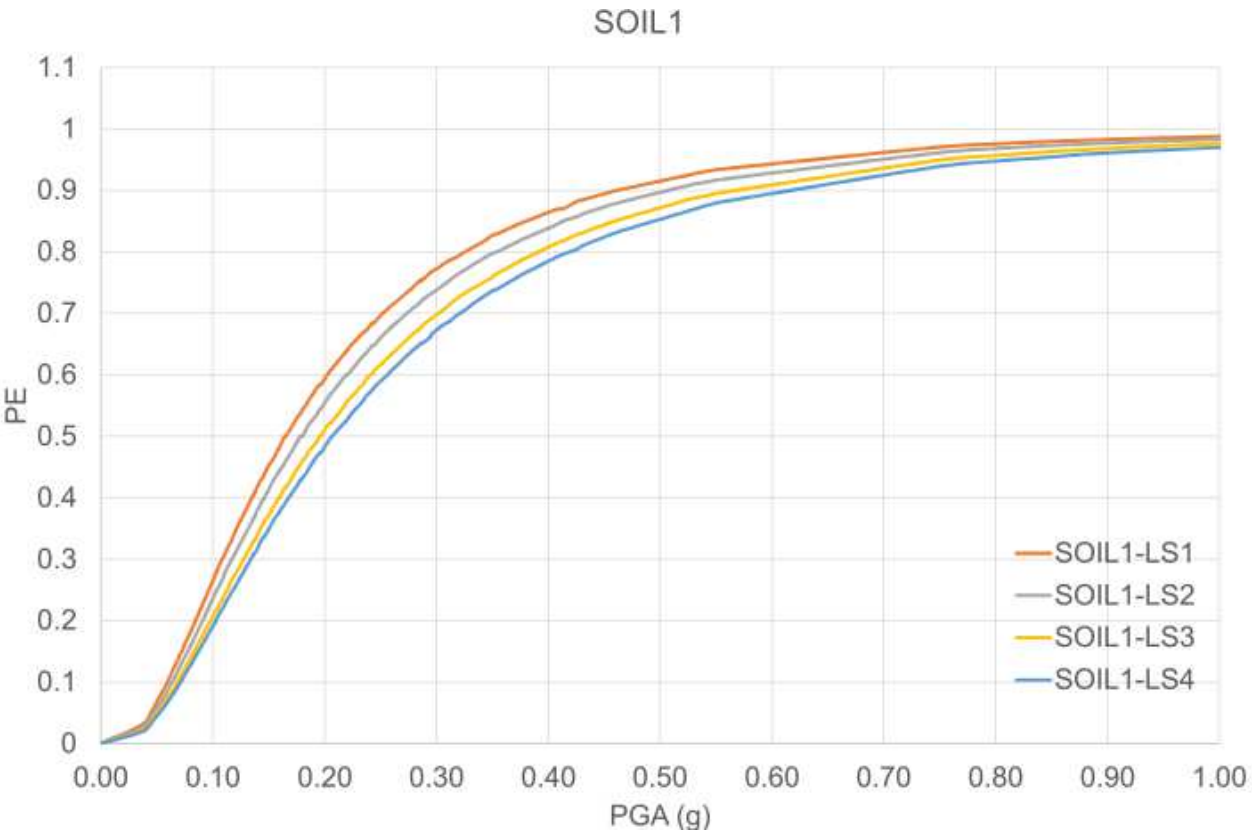

Fig. 6. Fragility Curves: SOIL 1

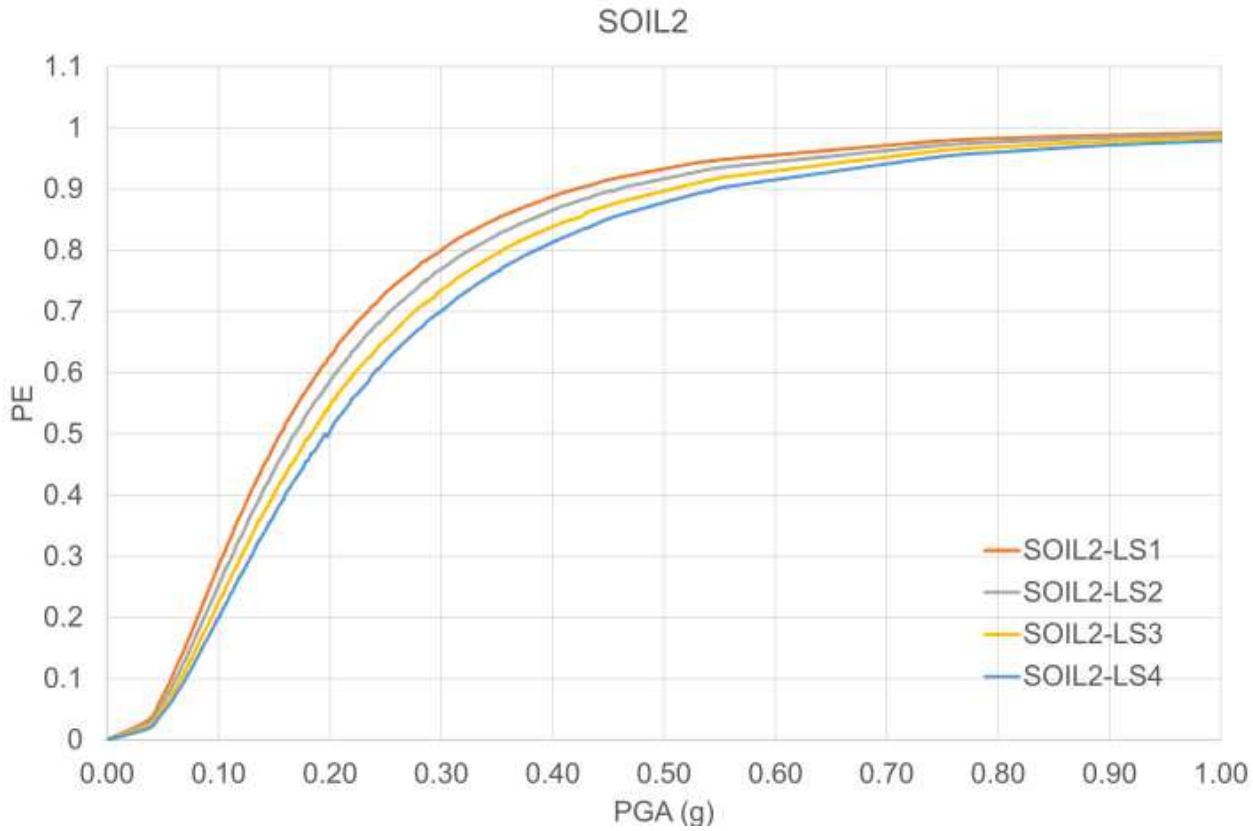

Fig. 7. Fragility Curves: SOIL 2

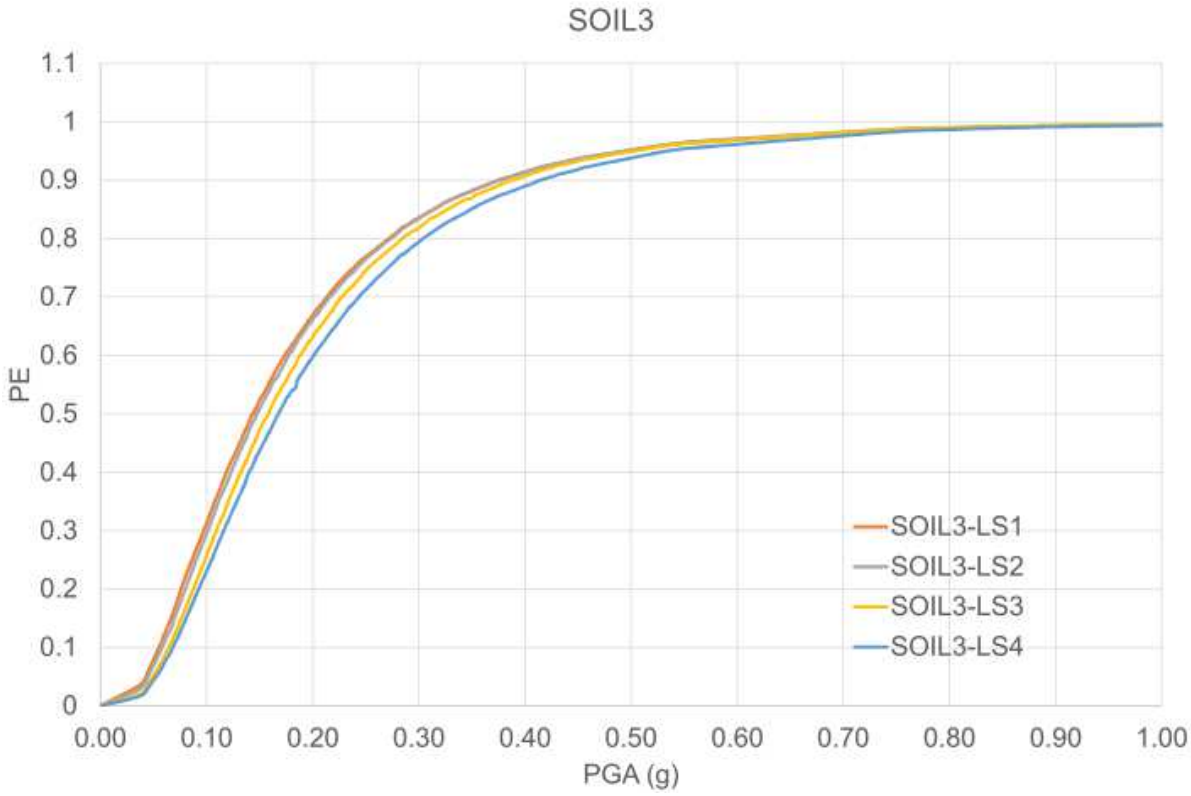

Fig. 8. Fragility Curves: SOIL 3

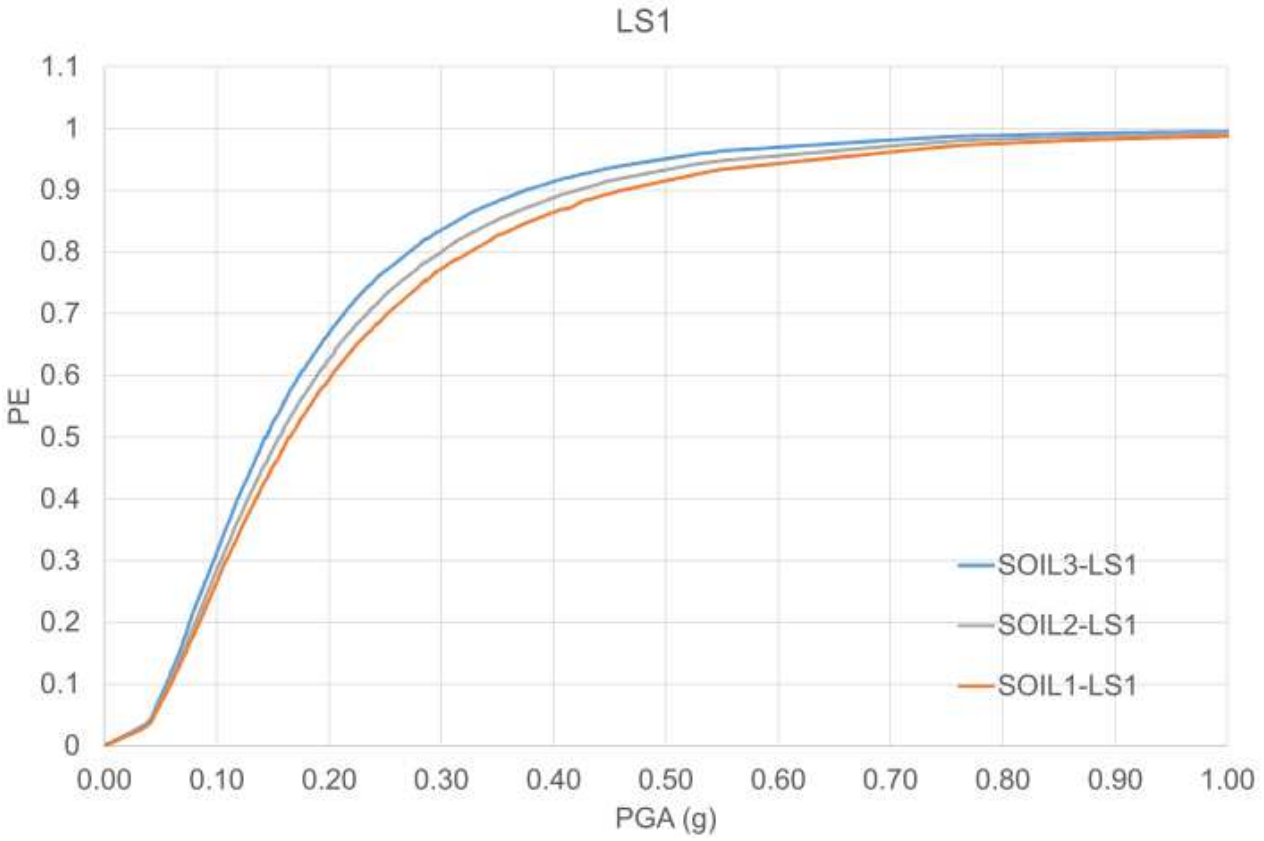

Fig. 9. Fragility curves: comparison LS1

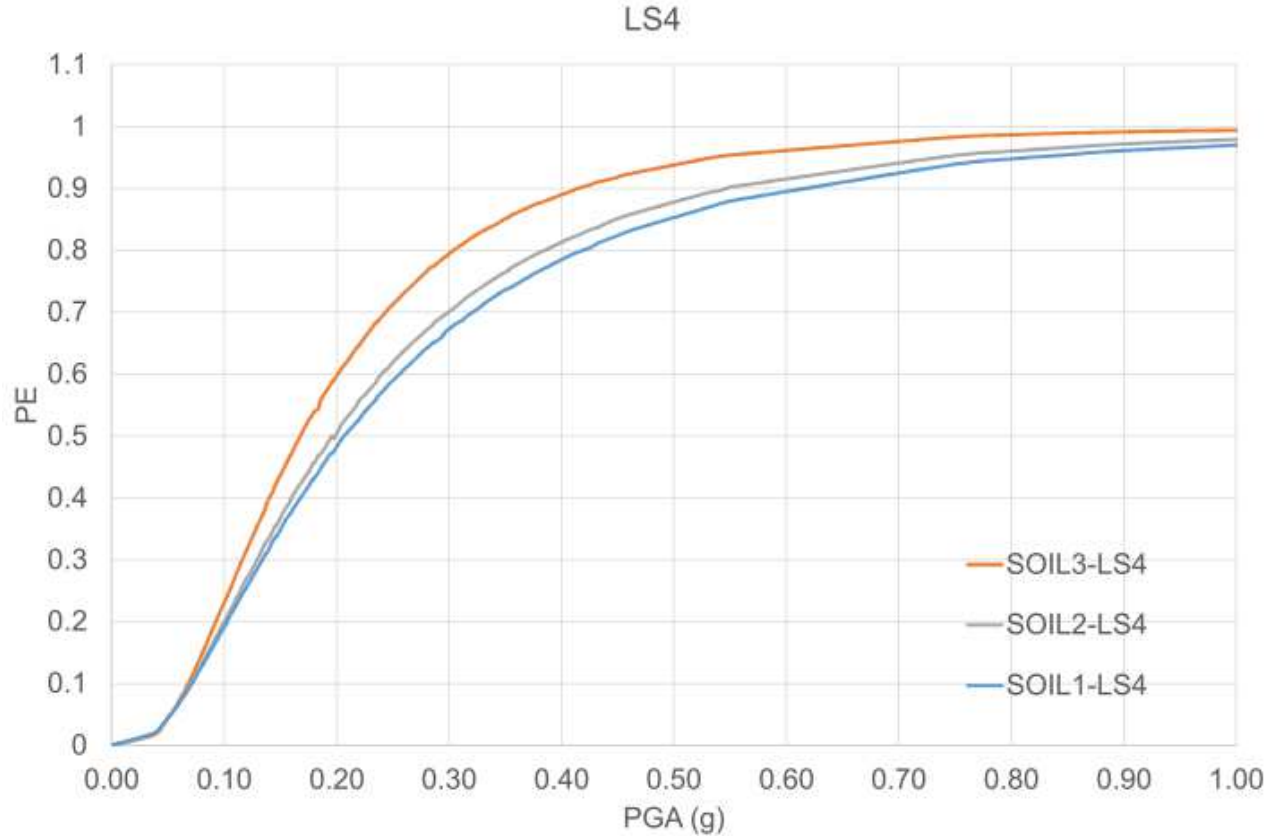

Fig. 10. Fragility curves: comparison LS4

Table 4. Lognormal standard deviation (β) and median (μ) values of SOIL1 at limit states (LSi).

SOIL1	LS1	LS2	LS3	LS4
β	0.793	0.809	0.821	0.833
μ	0.165g	0.176g	0.196g	0.207g

Table 5. Lognormal standard deviation (β) and median (μ) values of SOIL2 at limit states (LSi).

SOIL2	LS1	LS2	LS3	LS4
β	0.776	0.781	0.791	0.799
μ	0.156g	0.169g	0.183g	0.196g

Table 6. Lognormal standard deviation (β) and median (μ) values of SOIL3 at limit states (LSi).

SOIL1	LS1	LS2	LS3	LS4
β	0.749	0.728	0.670	0.705
μ	0.144g	0.149g	0.158g	0.168g

Table 7. PE at PGA=0.30 g for various soil conditions and limit states.

PGA=0.30g	LS1	LS2	LS3	LS4
SOIL1	0.77	0.73	0.70	0.68
SOIL2	0.80	0.78	0.72	0.70
SOIL3	0.84	0.83	0.81	0.79

CONCLUSIONS

A numerical model was validated and was used to study the interaction between earthquake actions and the response of a unburied subsea pipeline. In order to do so, a steel pipeline with OD/t = 20 laid on a sleeper with h/OD = 1.97 was considered. Different soil conditions with variable deformability were performed. The results from the 300 (100 for the 3 soil conditions) dynamic analyses were represented in order to build linear regression and define the mean and log-standard deviation values. The FE model was firstly validated by comparing the results with the ones calculated in the previous study (Mina et al., 2020) for the case of SOIL1. The results show a good agreement, meaning that the

model assumptions were properly defined. The conditions of rigid soil (no SSI) were compared with the other soil conditions. It is worth noting that deformable soils (SOIL2 and SOIL3) showed smaller mean values than those for SOIL1, underlining the effect of soil deformability in reducing the seismic vulnerability of the soil-pipeline system. In particular, the non-linear behaviour of the soil was driven by the ultimate strength of the soil that needs a certain level of intensity to be mobilized. Therefore, the relative damage of the two soil conditions differ mainly at moderate level of PGA because such intensities may affect the soil in different ways. It was found that at high level of PGA, the soil mobilizes plastic behaviour affecting the performance of the soil-pipeline system. The most deformable soil (SOIL3) showed larger values of PE, demonstrating that SSI effects are detrimental. Overall, the paper showed how the strains due to scenario 1 (Mina et al., 2020) may considerably be amplified when soil deformation vary. It was shown that neglecting the SSI effects on the performance of the system (stiff soil conditions) may considerably undervalue the pipeline vulnerability, leading to unconservative predictions and designs. The proposed findings may be included in code provisions to consider the role of SSI with a probabilistic-based approach

DECLARATIONS

Funding this research was not supported by any funds.

Conflicts of interest/Competing interests the authors have no conflict of interests nor competing ones.

Availability of data and material Data and material are available.

Code availability Opensees is regularly available to the writers.

REFERENCE

Alrsai, M., & Karampour, H. (2016, October). Propagation buckling of pipe-in-pipe systems, an experimental study. In The Twelfth ISOPE Pacific/Asia Offshore Mechanics Symposium. International Society of Offshore and Polar Engineers.

Arifin RB, Shafrizal WM, Wan B, Yusof M, Zhao, P, Bai Y. Seismic analysis for the subsea pipeline system. In: Proceedings of the ASME 2010 29th international conference on ocean, offshore and arctic engineering, OMAE2010-20671, Shanghai, China; 2010.

Binazir, A., Karampour, H., Sadowski, A. J., & Gilbert, B. P. (2019). Pure bending of pipe-in-pipe systems. Thin-Walled Structures, 145, 106381.

Daiyan N, Kenny S, Phillips R, Popescu R. Numerical investigation of oblique pipeline/soil interaction in sand. In: Proceedings of the 8th international pipeline conference, IPC2010-31644, Calgary, Alberta, Canada; 2010.

Dyan J, Kyriakides S. On the response of elastic-plastic tubes under combined bending and tension. J Offshore Mech Arctic Eng 1992;114(1):50–62.

Forcellini D. (2020a) Soil-structure interaction analyses of shallow-founded structures on a potential-liquefiable soil deposit. Soil Dynam Earthq Eng 2020;133:106108. 2020.

[33] DNV-OS-F101 (2007)

Forcellini D. (2020b) Probabilistic-Based Assessment of Liquefaction-Induced Damage with Analytical Fragility Curves. Geosciences 2020, 10(8), 315; https://doi.org/10.3390/geosciences10080315

Forcellini D. (2021) Analytical fragility curves of shallow-founded structures subjected to Soil-Structure Interaction (SSI) effects. Soil Dynam Earthq Eng, 2021; 141:106487

Joshi S, Prashant A, Deb A, Jain SK. Analysis of buried pipelines subjected to reverse fault motion.

289 Soil Dynam Earthq Eng 2011;31(7):930–40. https://doi.org/10.1016/j.soildyn.2011.02.003.

290 Karamitros DK, Bouckovalas GD, Kouretzis GP. Stress analysis of buried steel pipelines at strike-
291 slip fault crossings. Soil Dynam Earthq Eng 2007;27(3):200–
292 11. https://doi.org/10.1016/j.soildyn.2006.08.001.

293 Karampour H., Albermani F., Gross J. On lateral and upheaval buckling of subsea pipelines. Eng
294 Struct 2013;52:317–330.

295 Karampour, H., Albermani, F., & Major, P. (2015, May). Interaction between lateral buckling and
296 propagation buckling in textured deep subsea pipelines. In International Conference on Offshore
297 Mechanics and Arctic Engineering (Vol. 56499, p. V003T02A079). American Society of Mechanical
298 Engineers.

299 Karampour, H., Wu, Z., Lefebure, J., Jeng, D. S., Etemad-Shahidi, A., & Simpson, B. (2018).
300 Modelling of flow around hexagonal and textured cylinders. Proceedings of the Institution of Civil
301 Engineers-Engineering and Computational Mechanics, 171(3), 99-114.

302 Karampour H. Effect of proximity of imperfections on buckle interaction in deep subsea pipelines.
303 Mar Struct 2018;59:444–457.

304 Kokavessis N, Anagnostidis G. Finite element modelling of buried pipelines subjected to seismic
305 loads: soil structure interaction using contact elements. In: Proceedings, ASMEPVP conf. Vancouver.
306 Canada: BC; 2006.

307 Lillig DB, Newbury BD, Altstadt SA. The second ISOPE strain-based design symposium—a review.
308 In: Proceedings of the international society of offshore & polar engineering conference, Osaka, Japan;
309 2009.

310 Liu A, Hu Y, Zhao F, Li X, Takada S, Zhao L. An equivalent-boundary method for the shell analysis
311 of buried pipelines under fault movement. Acta Seismol Sin 2004; 17:150–
312 6. https://doi.org/10.1007/s11589-004-0078-1.

313 Liu M, Wang Y, Yu Z. Response of pipelines under fault crossing. In: Proc. Int. offshore polar Eng.
314 Conf. Vancouver, BC: Canada; 2008.

315 Lu, J., Elgamal, A., & Yang, Z. (2011). OpenSeesPL: 3D lateral pile-ground interaction user manual
316 (Beta 1.0). Department of Structural Engineering, University of California, San Diego

317 Mazzoni S., McKenna F., Scott M.H., Fenves G.L. Open system for earthquake engineering
318 simulation, user command-language manual. Berkeley: Pacific Earthquake Engineering Research
319 Center, University of California; 2009. OpenSees version 2.0
320 http://opensees.berkeley.edu/OpenSees/manuals/usermanual.

321

322 Mina D., Forcellini D., Karampour H. Analytical fragility curves for assessment of the seismic
323 vulnerability of hp/ht unburied subsea pipelines. Soil Dynamics and Earthquake Engineering 137
324 (2020) 106308 2020.

325 Odina L, Tan R. Seismic fault displacement of buried pipelines using continuum finite element
326 methods. In: ASME 2009 28th int. Conf. Ocean. Offshore arct. Eng. Honolulu, Hawaii, USA.

327 Odina L, Conder RJ. Significance of Lüder's plateau on pipeline fault crossing assessment,
328 Proceedings of the ASME 2010 29th international conference on ocean, offshore and arctic
329 engineering, OMAE2010-20715, Shanghai, China; 2010.

330 Piran, F., Karampour, H., & Woodfield, P. (2020). Numerical Simulation of Cross-Flow Vortex-
331 Induced Vibration of Hexagonal Cylinders with Face and Corner Orientations at Low Reynolds
332 Number. Journal of Marine Science and Engineering, 8(6), 387.

333 Shitamoto H, Hamada M, Okaguchi S, Takahashi N, Takeuchi I, Fujita S. Evaluation of compressive
334 strain limit of X80 SAW pipes for resistance to ground movement. In: Proceedings of the twentieth
335 international offshore and polar engineering conference, Beijing, China; 2010.

336 Stephan, P., Love, C., Albermani, F., & Karampour, H. (2016). Experimental study on confined
337 buckle propagation. Advanced Steel Construction, 12(1), 44-54.

338 Thebian L, Najjar S, Sadek S, Mabsout M. Finite element analysis of offshore pipelines overlying
339 active reverse fault rupture. Proc Int Conf Offshore Mech Arct Eng - OMAE
340 2017;9. https://doi.org/10.1115/OMAE2017-61496.

341 Triantafyllaki A, Papanastasiou P., Loukidis D. Numerical analysis of the structural response of
342 unburied offshore pipelines crossing active normal and reverse faults Soil Dynamics and Earthquake
343 Engineering 137 (2020) 106296

344 Vazouras P, Karamanos SA, Dakoulas P. Mechanical behavior of buried steel pipes crossing active
345 strike-slip faults. Soil Dynam Earthq Eng 2012; 41:164–80.
346 https://doi.org/10.1016/j.soildyn.2012.05.012.

347 Vazouras P, Dakoulas P, Karamanos SA. Pipe-soil interaction and pipeline performance under strike-
348 slip fault movements. Soil Dynam Earthq Eng 2015;72:48–
349 65. https://doi.org/10.1016/j.soildyn.2015.01.014.

350 Vazouras P, Karamanos SA, Dakoulas P. Finite element analysis of buried steel pipelines under
351 strike-slip fault displacements. Soil Dynam Earthq Eng 2010; 30 (11):1361–
352 76. https://doi.org/10.1016/j.soildyn.2010.06.011.

353 Yun H, Kyriakides S. On the beam and shell modes of buckling of buried pipelines. Soil Dynam
354 Earthq Eng 1990;9(4):179–93. https://doi.org/10.1016/S0267-7261 (05)80009-0.

355 Zhang J, Liang Z, Han CJ. Buckling behavior analysis of buried gas pipeline under

356 strike-slip fault displacement. J Nat Gas Sci Eng 2014;21:921–8. https://doi.org/

357 10.1016/j.jngse.2014.10.028.

358

Figures

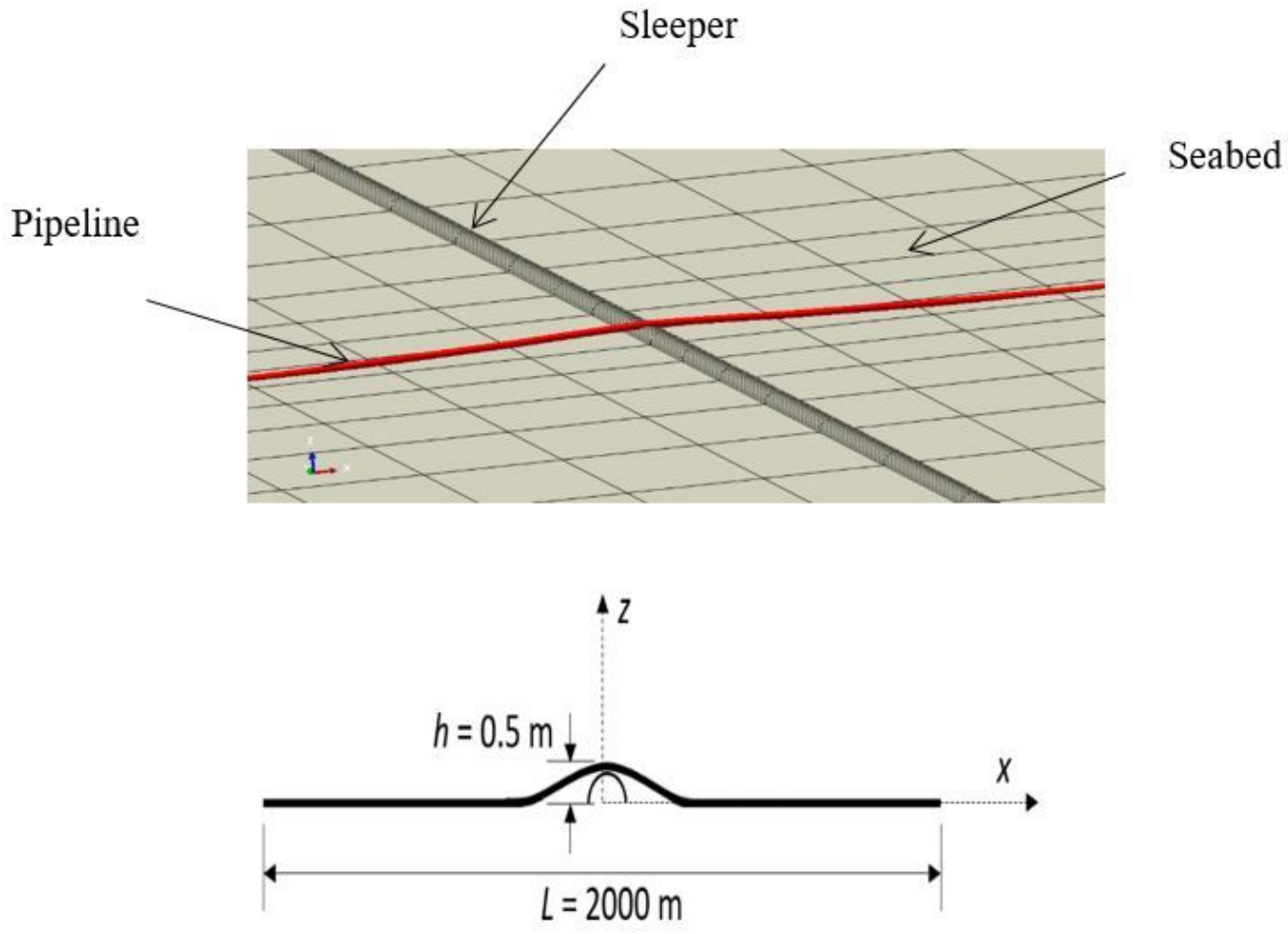

Figure 1

Pipeline and sleeper model used in the thermal buckling and seismic/thermal interaction analyses in Mina et al. (2020).

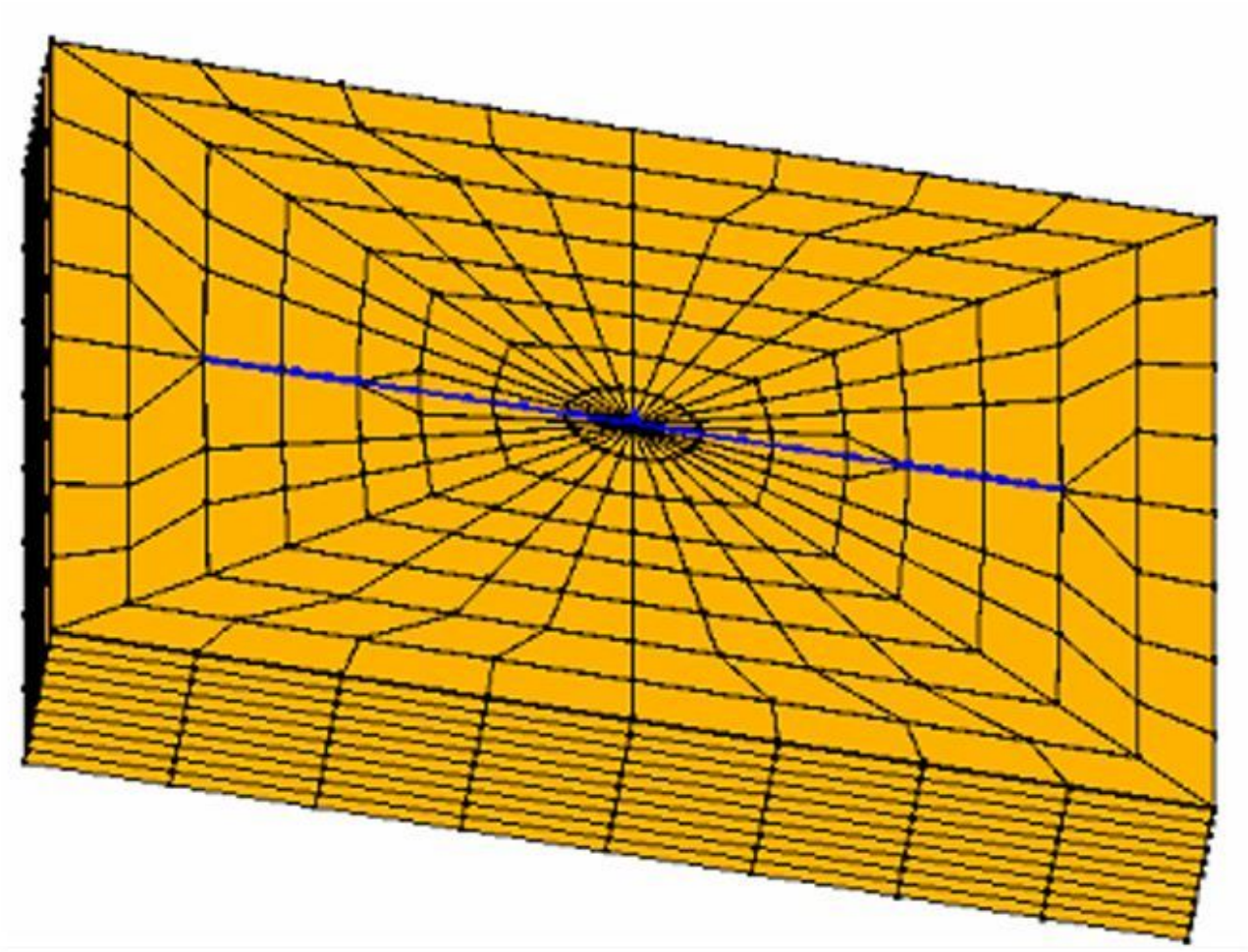

Figure 2

The finite element mesh

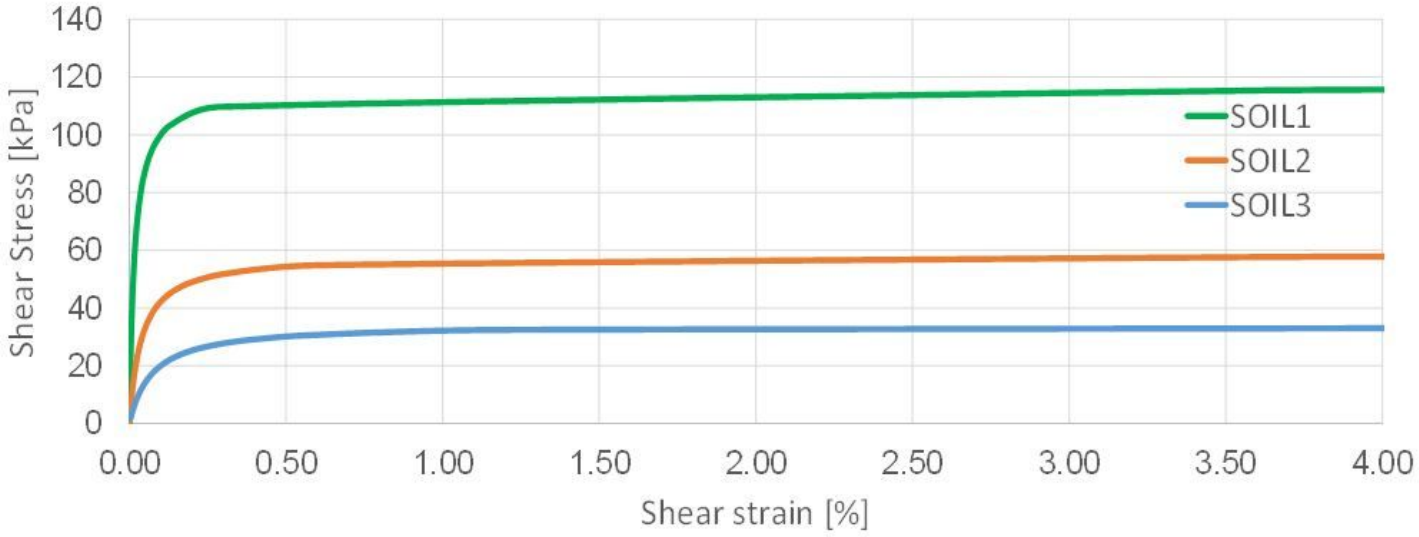

Figure 3

Backbone curves

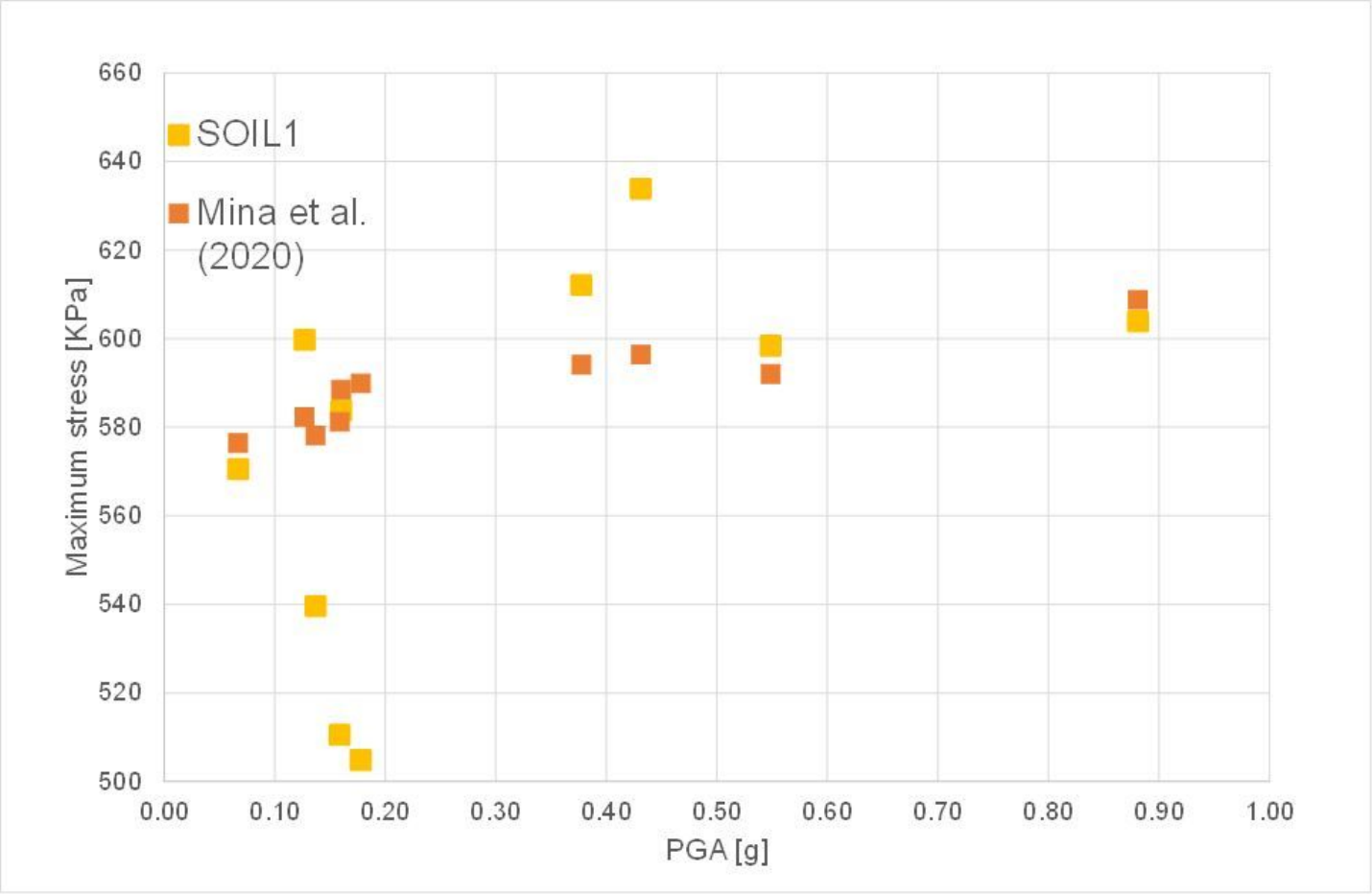

Figure 4

Comparison: Mina et al. (2020) and Soil 1 results

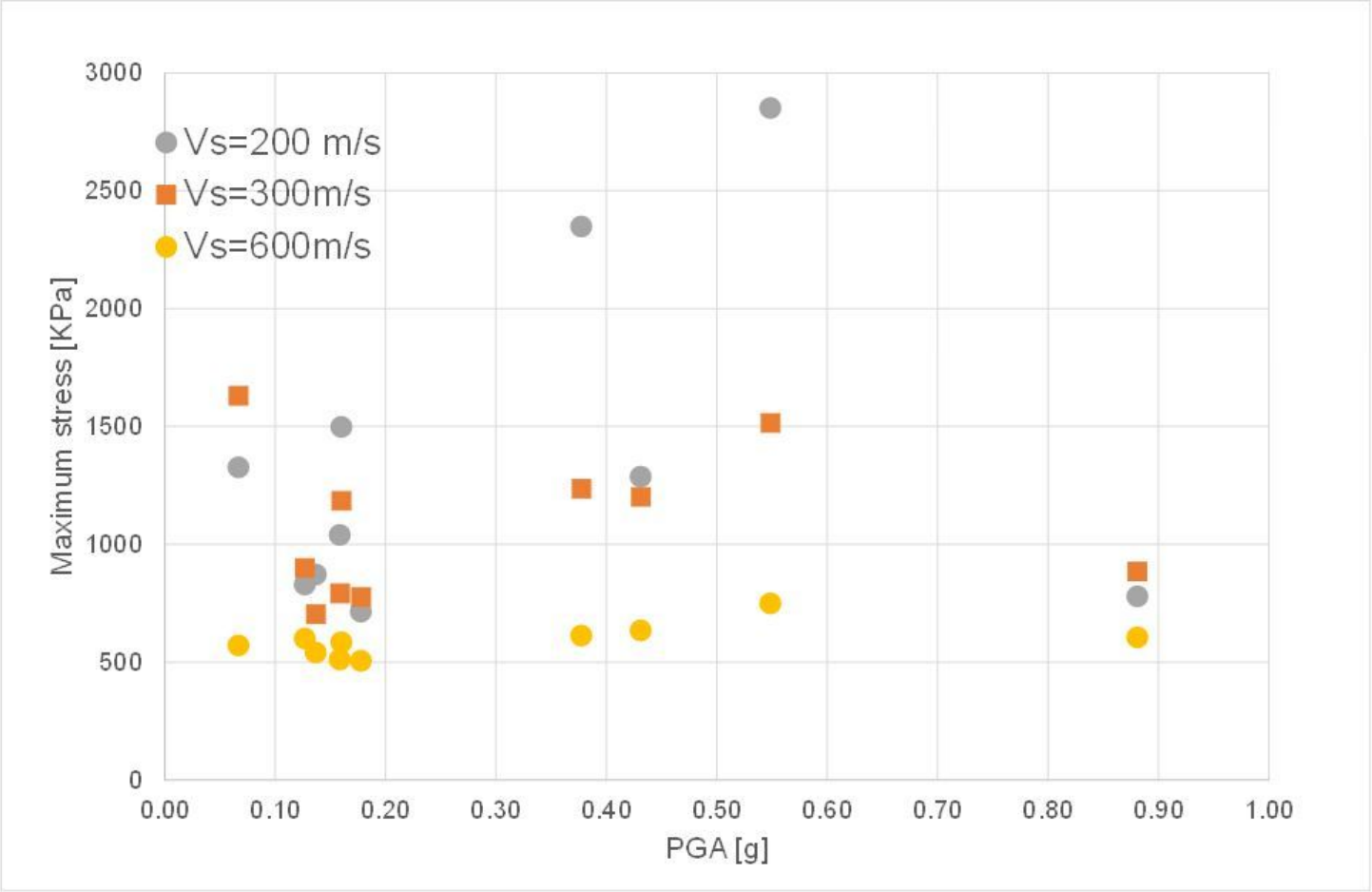

Figure 5

Comparison: SSI effects

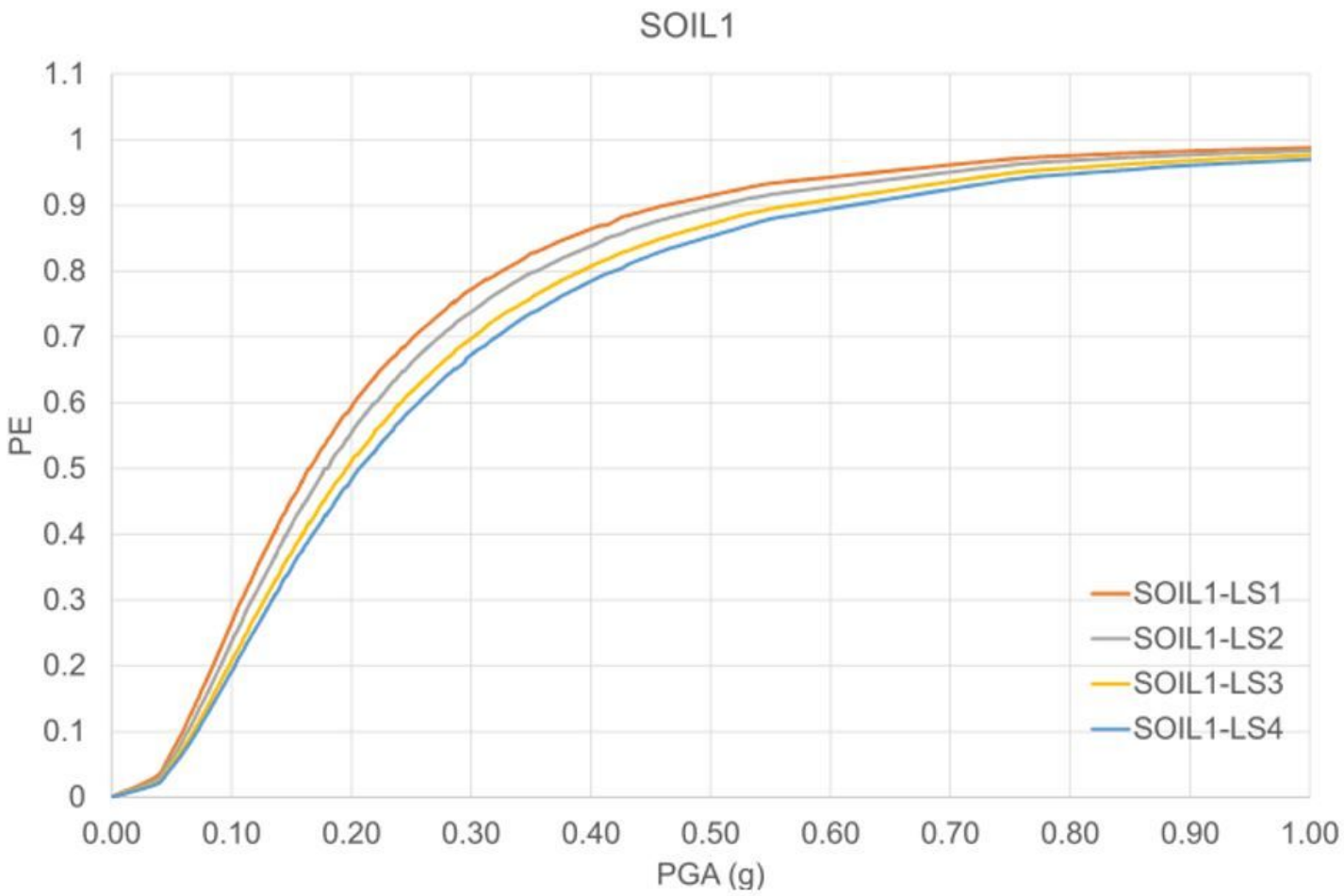

Figure 6

Fragility Curves: SOIL 1

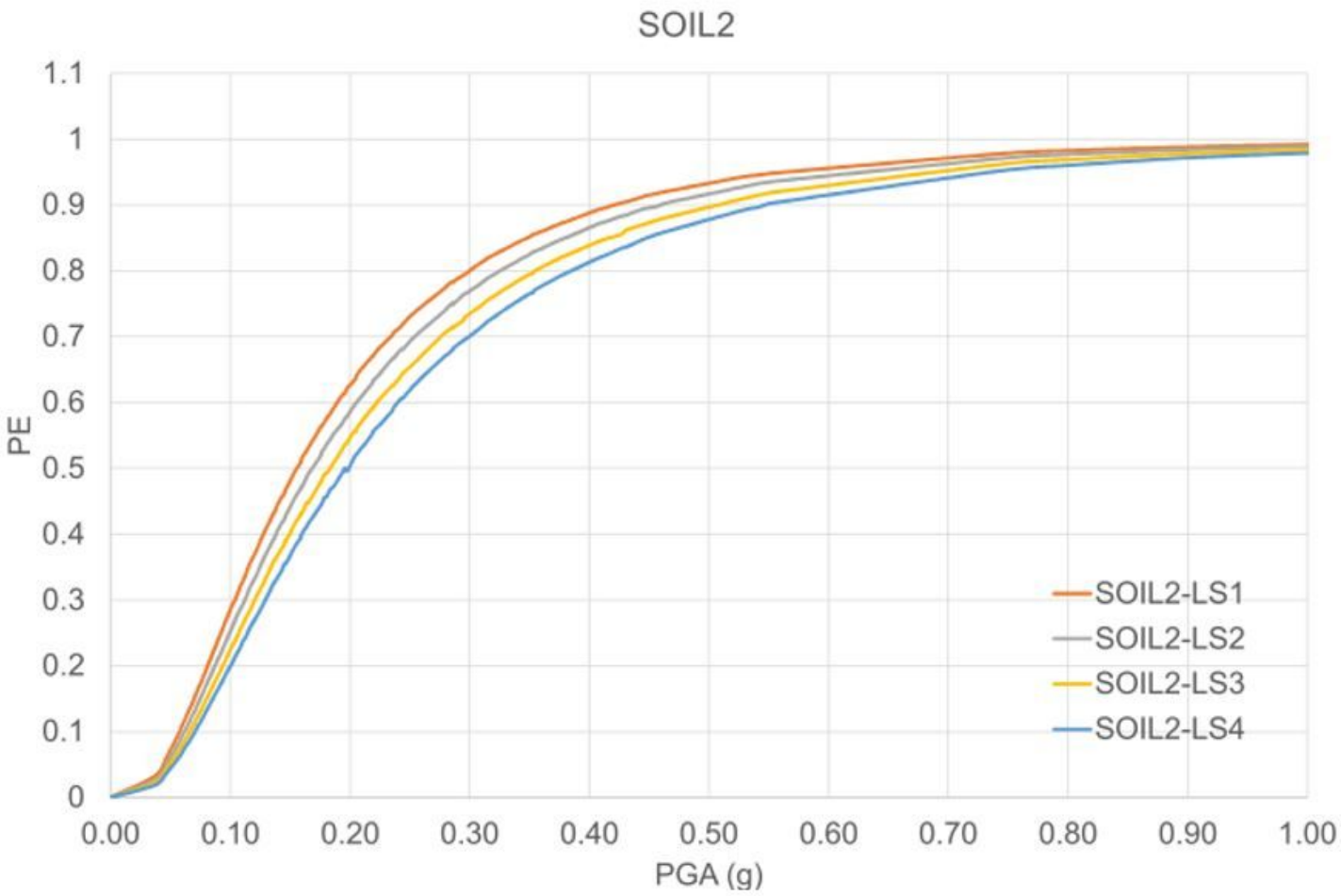

Figure 7

Fragility Curves: SOIL 2

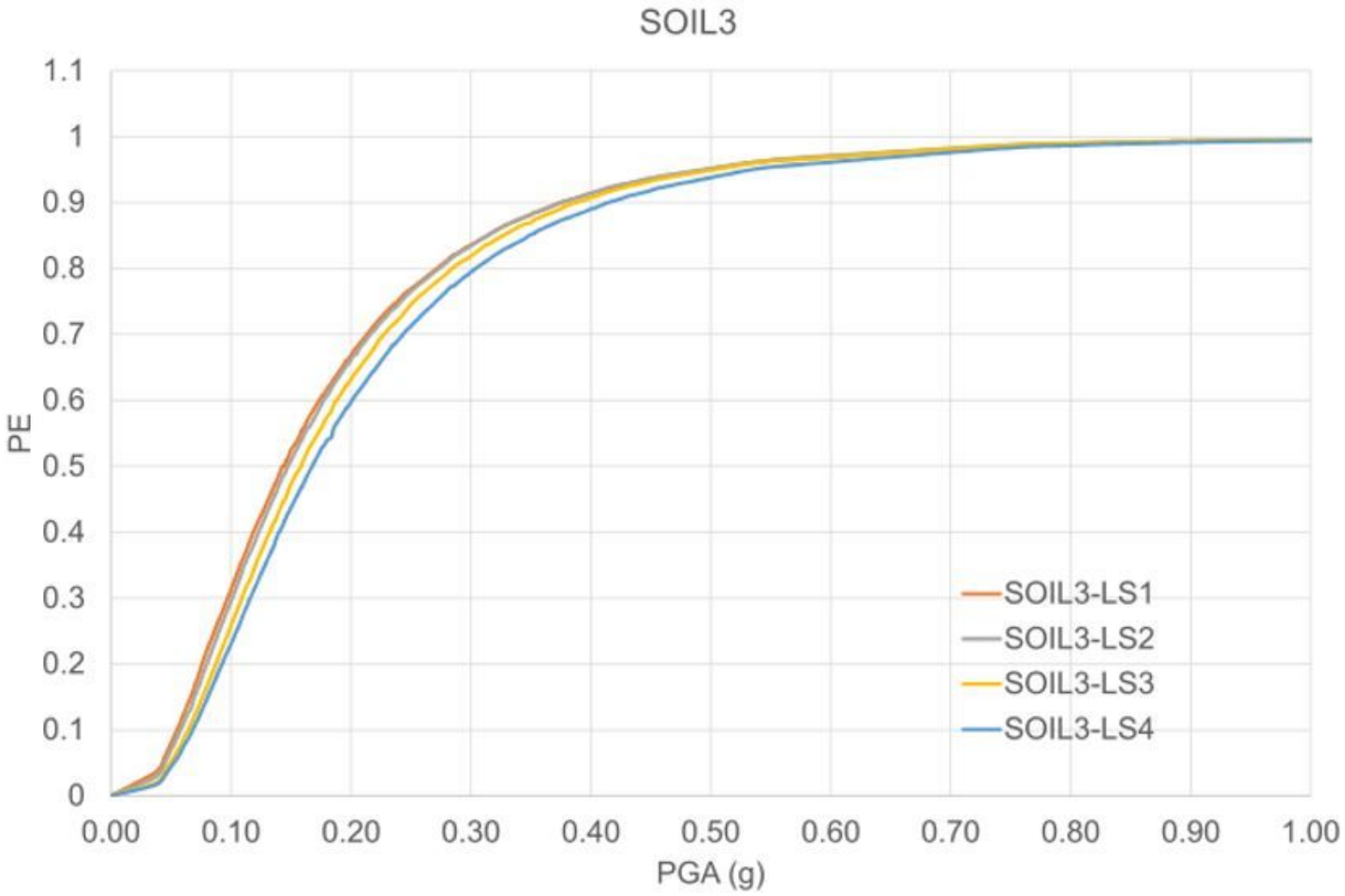

Figure 8

Fragility Curves: SOIL 3

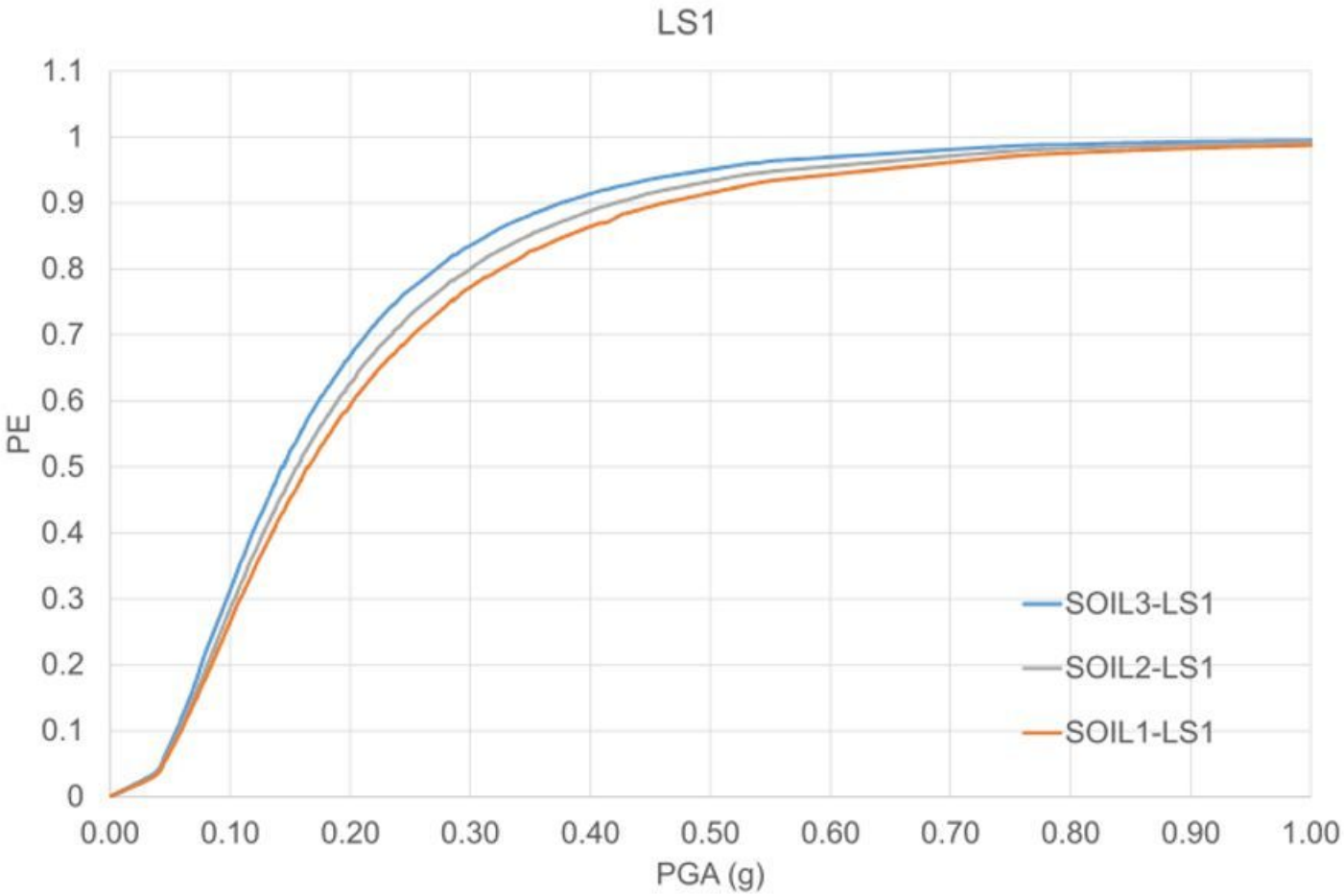

Figure 9

Fragility curves: comparison LS1

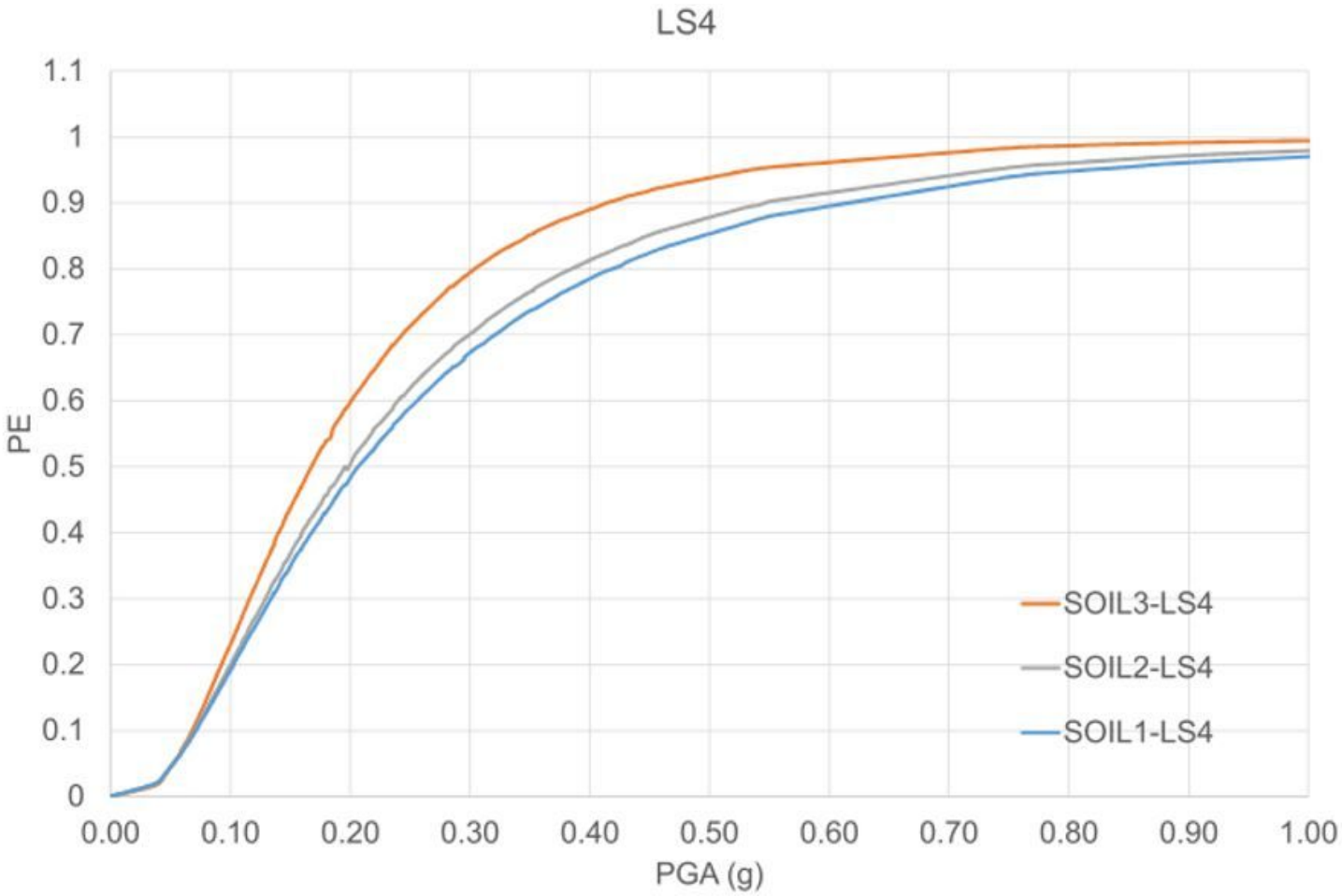

Figure 10

Fragility curves: comparison LS4